Supporting Information

Size-Dependent Photothermal Conversion and Photoluminescence of Theranostic $NaNdF_4$ Nanoparticles under Excitation of Different-Wavelength Lasers

*Lihua Ding, Feng Ren, Zheng Liu, Zhilin Jiang, Baofeng Yun, Qiao Sun, Zhen Li**

Center for Molecular Imaging and Nuclear Medicine, State Key Laboratory of Radiation Medicine and Protection, School for Radiological and Interdisciplinary Sciences (RAD-X), Soochow University, Collaborative Innovation Center of Radiation Medicine of Jiangsu Higher Education Institutions
Suzhou 215123, China
Email: zhenli@suda.edu.cn

Calculation of the photothermal conversion efficiency

1 mL of 6 mg/mL NNF-P NPs solution was loaded into a silica dish and then continuously irradiated by an 808 nm laser, until it reached a steady-state temperature, the solution was naturally cooled after the laser was turned off. The monitored temperature profile is shown in Figure S6. The photothermal conversion efficiency (η) was calculated on the basis of the following equation.

$$\eta = \frac{hS(T_{max} - T_{surr}) - Q_0}{I(1 - 10^{-A_{808}})} \quad (1)$$

where h is the heat transfer coefficient, S is the surface area of the sample container, T_{max} (59.8 °C) is the equilibrium temperature, T_{surr} (31 °C) is the ambient temperature of the surroundings, Q_0 represents the heat dissipation from the light absorbed by the quartz sample cell, I is the incident laser power (750 mW), and A_{808} (0.23816) is the absorbance of the NNF-P NPs at 808 nm. The value of hS is derived on the basis of the following equation:

$$\tau_s = \frac{m_d C_d}{hS} \quad (2)$$

where m is the solution mass and equal to 1.0 g in the current study, c is the heat capacity of water and equal to 4.2 J/g, therefore, the time constant is linearly fitted to be τs = 401.583 s, according to the linear time relationship from the cooling profile (refer to Figure S6c). Based on Eq. (2), h is deduced to be 10.45 mW/°C.

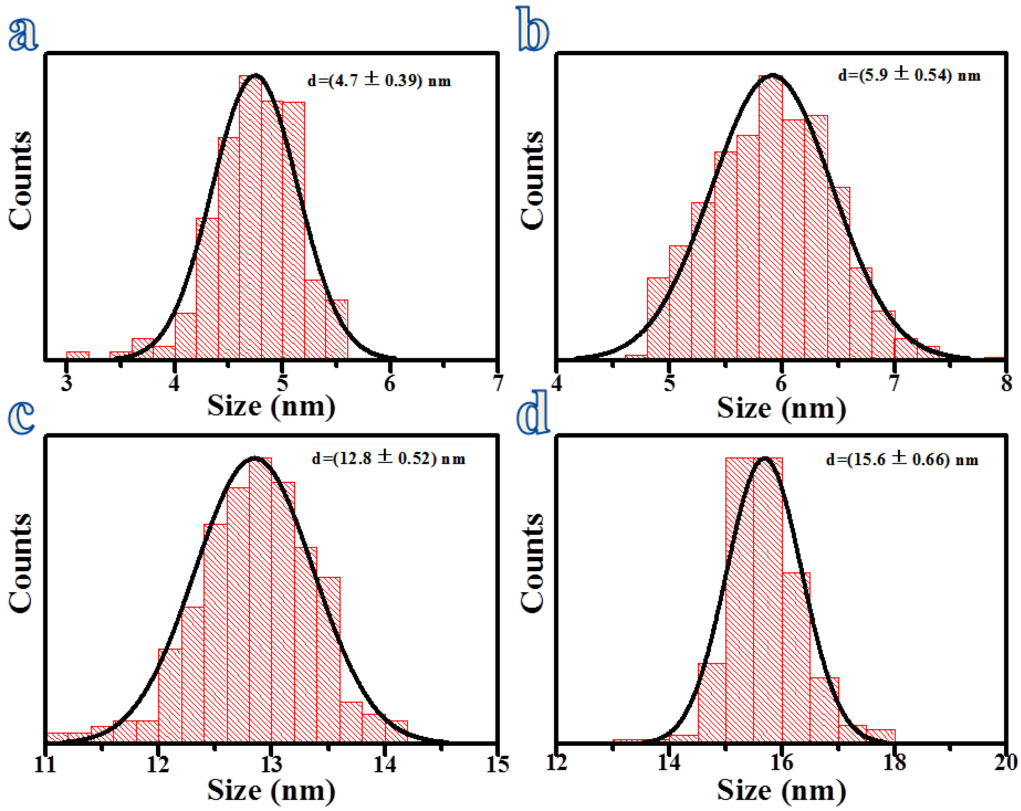

Figure S1. The corresponding size distributions of different sized NNF NPs shown in Figure 1 (a-d).

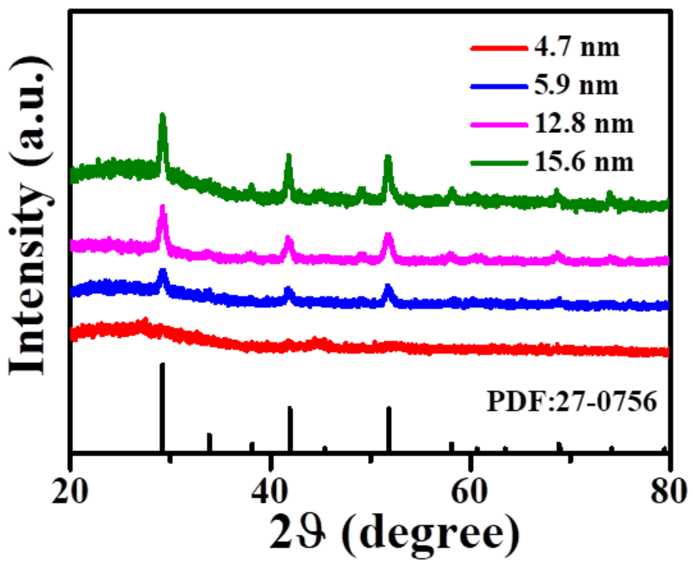

Figure S2. XRD patterns of different sized NNF NPs.

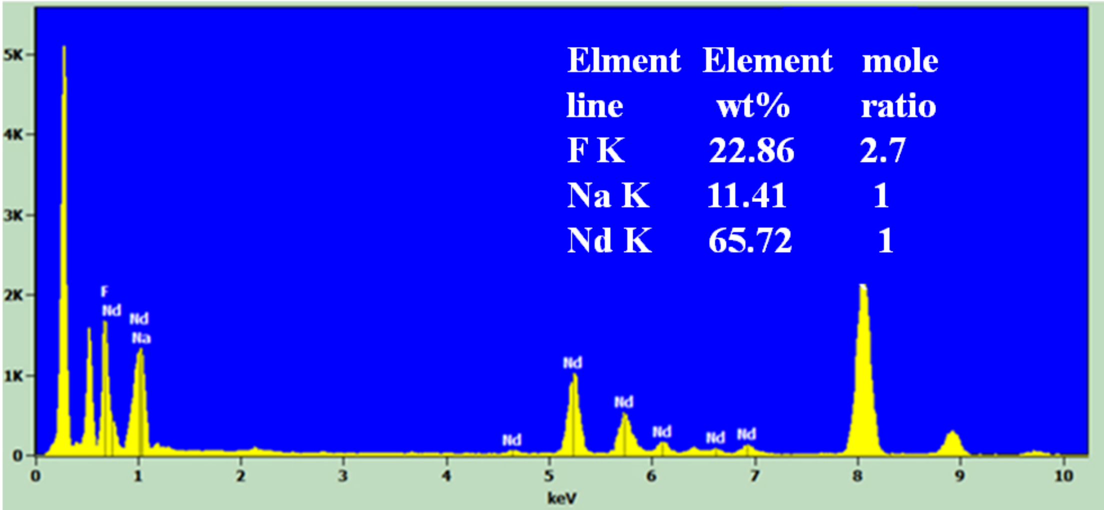

Figure S3. The EDX spectrum of 12.8 nm NNF NPs.

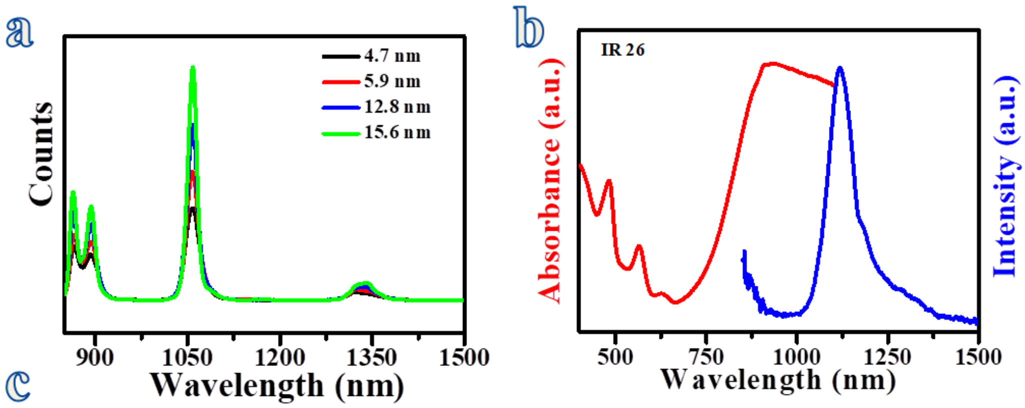

c

	A_{808}	QY (1060)	QY (1330)	QY (1060+1330)	QY (all)
IR 26	0.058525				0.5%
4.7 nm	0.05924	0.86%	0.16%	1.02%	1.71%
5.9 nm	0.055742	1.12%	0.20%	1.32%	2.17%
12.8 nm	0.052728	1.40%	0.24%	1.65%	2.74%
15.6 nm	0.048723	1.72%	0.30%	2.01%	3.29%

Figure S4. (a) Emission spectra of different sized NNF NPs under the 808 nm excitation. (b) Absorption and emission spectra (under 808 nm excitation) of Dye IR26 dispersed in dichloroethane. (c) The fluorescence quantum yields of different sized NNF NPs.

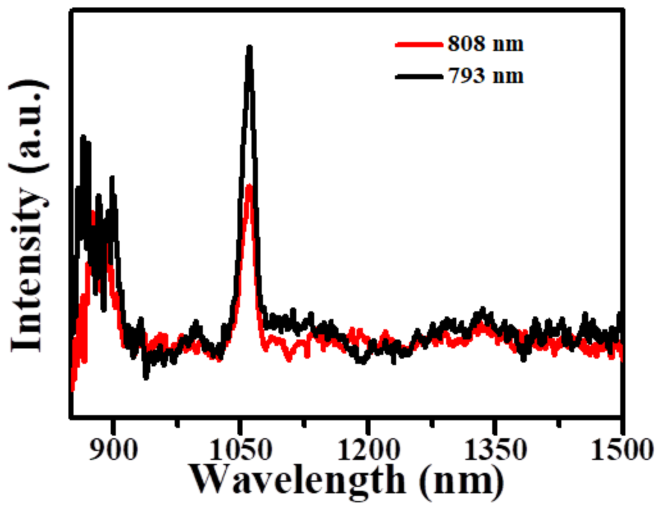

Figure S5. Emission spectra of NNF NPs under excitations by an 808 nm laser (red) and a 793 nm laser (black), respectively.

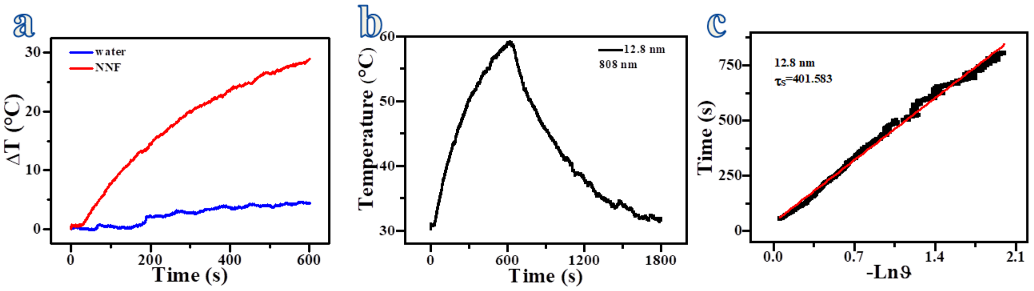

Figure S6. (a) Temperature curves of water and NNF-P NPs solution irradiated by an 808 nm laser with a power density of 0.75 W/cm^2. (b) The temperature profile of NNF-P NPs solution irradiated with the 808 nm laser, followed by natural cooling after the laser was turned off, (c) determination of the system time constant using linear regression of the cooling profile in (b).

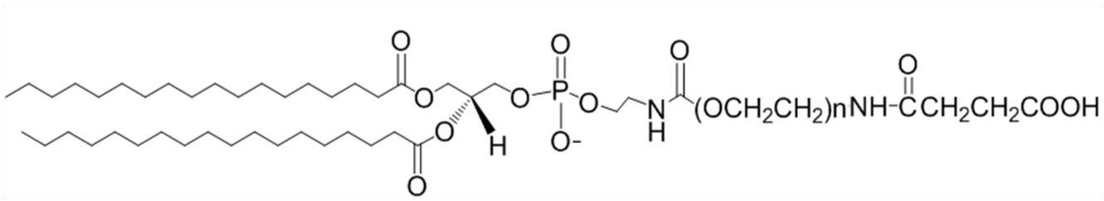

DSPE-PEG$_{5000}$-COOH

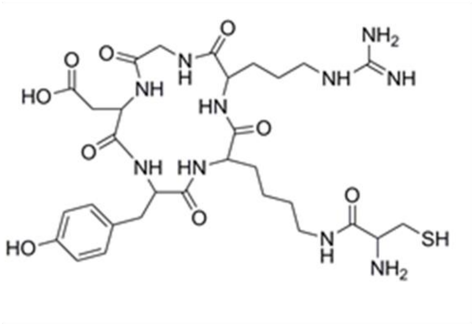

Arg-Gly-Asp-Tys-Cys

Figure S7. Chemical structures of the DSPE-PEG$_{5000}$–COOH and RGD peptide.

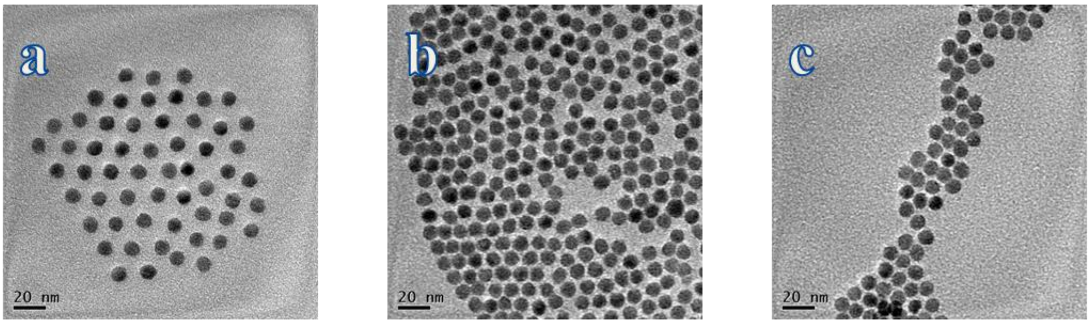

Figure S8. Transmission electron microscope (TEM) images of (a) NNF-P NPs, (b) NNF-P NPs after photothermal treatment, and (c) NNF-P-R NPs.

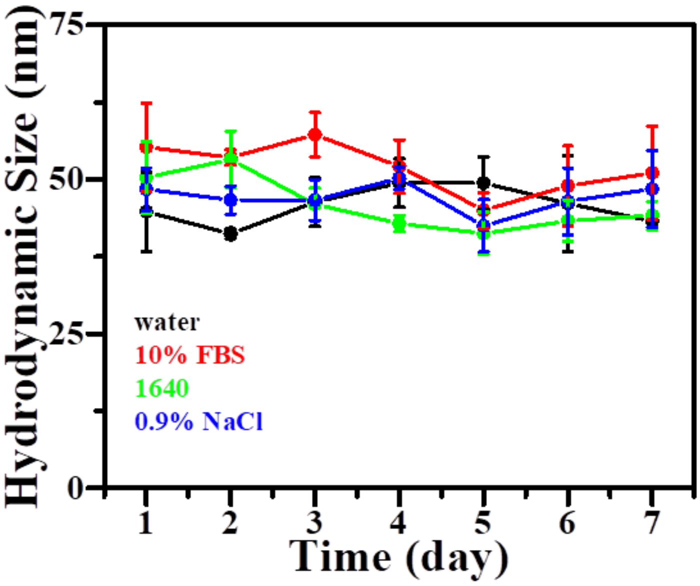

Figure S9. Variation of hydrodynamic size of NNF-P NPs stored in different solutions [water (black), 10 % FBS (red), 1640 (green), 0.9 % NaCl (blue)] for 7 days, respectively.

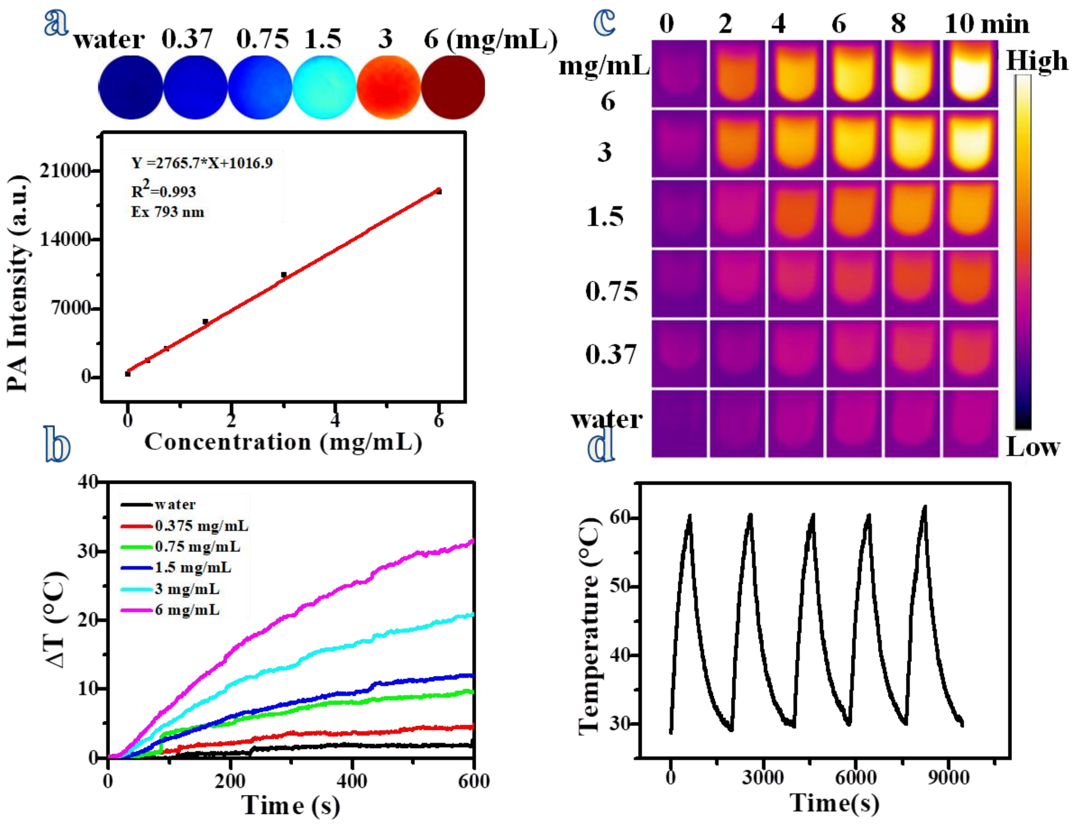

Figure S10. (a) The dependence photoacoustic (PA) intensity of NNF-P NPs on their concentrations under the excitation of the 793 nm laser, with the inset showing PA images of different concentrations of nanoparticles, respectively. (b) Temperature curves and (c) photothermal images of different concentrations of NNF-P NPs. (d) Heating and cooling profiles of an aqueous solution of NNF-P NPs under the irradiation by the 808 nm laser with a power density of 0.75 W/cm^2 for five cycles.

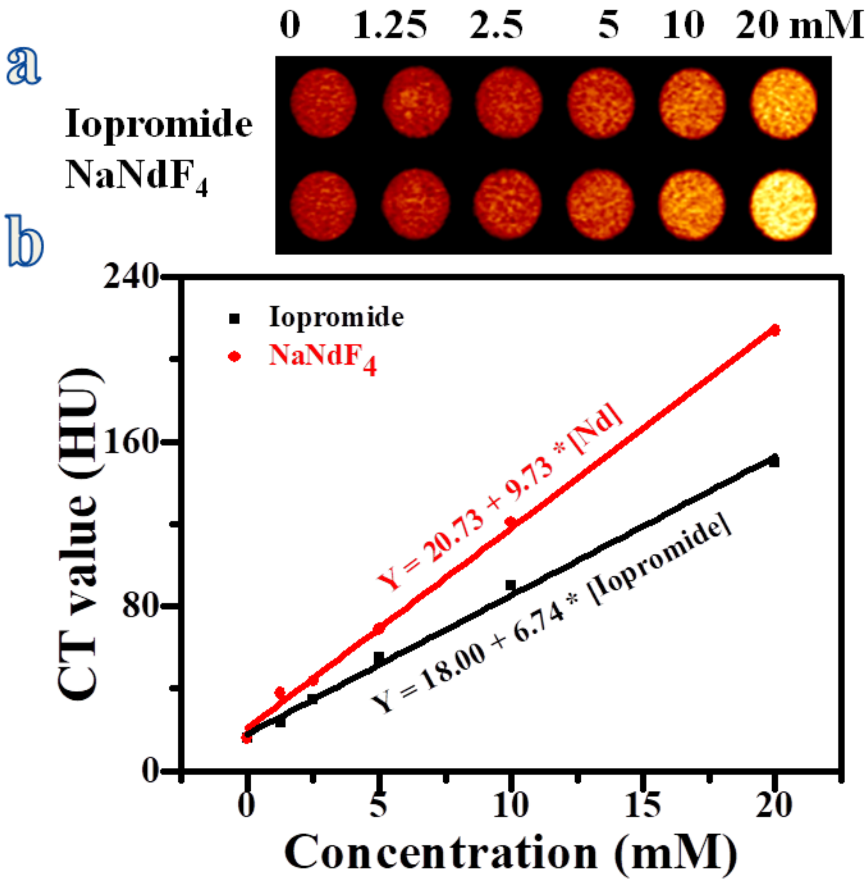

Figure S11. *In vitro* CT images and values obtained from different concentrations of our nanoparticles in comparison with clinical contrast agent iopromide.

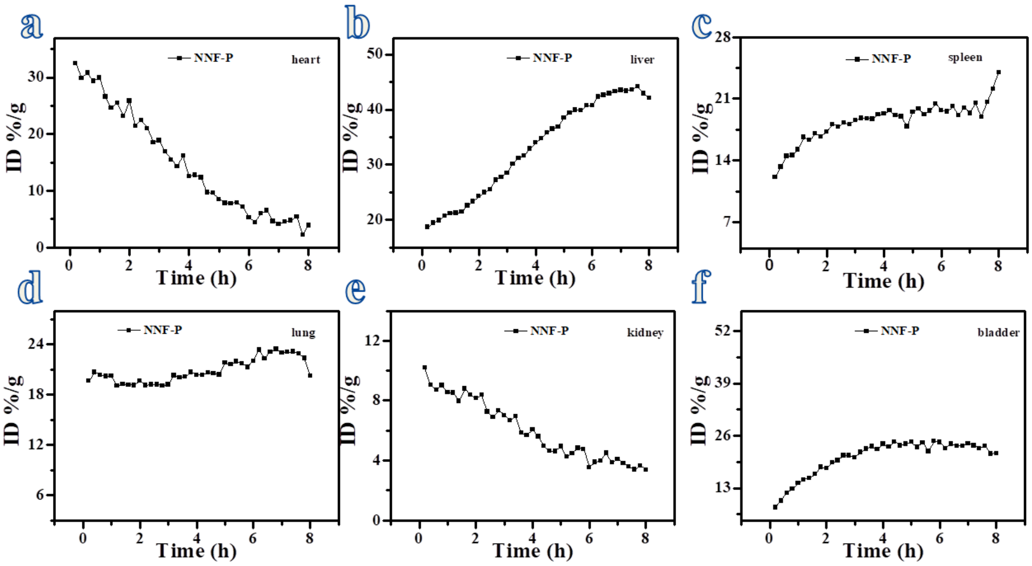

Figure S12. Biodistribution of nanoparticles quantified by counting the Gamma emissions in the SPECT/CT images of different organs, *i.e.*, (a) heart, (b) liver, (c) spleen, (d) lung, (e) kidney, and (f) bladder. The SPECT/CT images were taken at different times after intravenous injection of NNF-P-^{99m}Tc NPs solution into the mice.

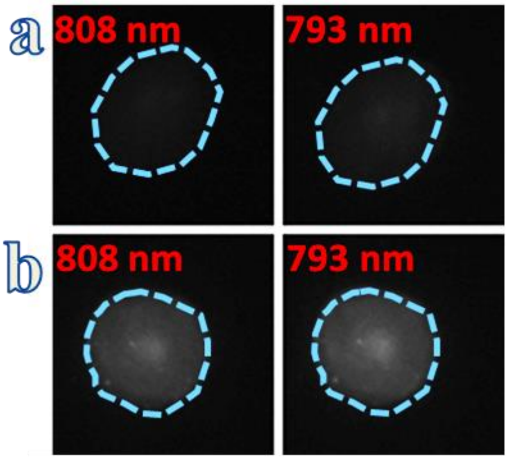

Figure S13. NIR-II fluorescence images of disserted tumor from the tumor-bearing mice: (a) injected with NNF-P NPs (b) injected with NNF-P-R NPs under the excitation of different lasers (left tumors were excited with the 808 nm laser, and the right ones were excited with the 793 nm laser, respectively).

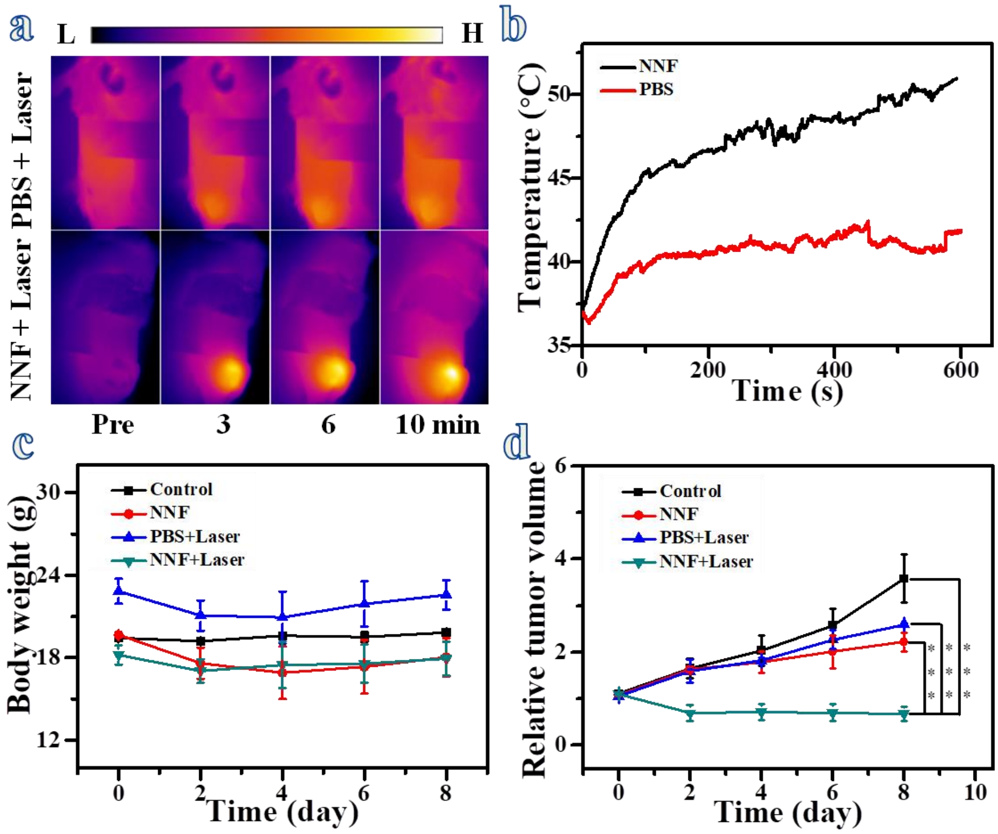

Figure S14. (a) Infrared thermal images of tumor-bearing mice and (b) the temperature curves of the tumors after they were intratumoral injected with NNF-P NPs (dose 6 mg/mL, 50 μL) and PBS, respectively, and then exposed to an 808 nm NIR laser (1 W/cm^2, 10 min). The variations in (c) weight, (d) relative tumor volume. (*p < 0.5, **p < 0.01, ***p < 0.001)

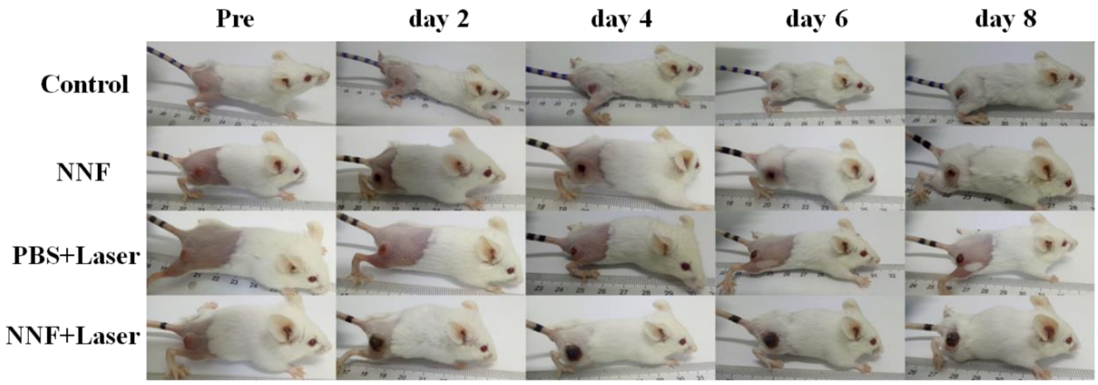

Figure S15. Photographs of the four groups of mice taken at different times after treatment: (1) control group, (2) NNF group, (3) PBS + Laser group, and (4) NNF + Laser group.